

NJC

Accepted Manuscript



This article can be cited before page numbers have been issued, to do this please use: M. Rahimi, R. Karimian, E. Mostafidi, E. B. Noruzi, S. Taghizadeh, B. Shokouhi and H. S. Samadi Kafil, *New J. Chem.*, 2018, DOI: 10.1039/C8NJ01790E.



This is an Accepted Manuscript, which has been through the Royal Society of Chemistry peer review process and has been accepted for publication.

Accepted Manuscripts are published online shortly after acceptance, before technical editing, formatting and proof reading. Using this free service, authors can make their results available to the community, in citable form, before we publish the edited article. We will replace this Accepted Manuscript with the edited and formatted Advance Article as soon as it is available.

You can find more information about Accepted Manuscripts in the [author guidelines](#).

Please note that technical editing may introduce minor changes to the text and/or graphics, which may alter content. The journal's standard [Terms & Conditions](#) and the ethical guidelines, outlined in our [author and reviewer resource centre](#), still apply. In no event shall the Royal Society of Chemistry be held responsible for any errors or omissions in this Accepted Manuscript or any consequences arising from the use of any information it contains.

Highly branched amine-functionalized p-sulfonatocalix[4]arene decorated with human plasma proteins as a smart, targeted, and stealth nano-vehicle for combination chemotherapy of MCF7 cells

Mahdi Rahimi ^{a, b}, Ramin Karimian ^{*c}, Elmira Mostafidi^d, Ehsan Bahojb Noruzi^e,
Sepehr Taghizadeh^f, Behrooz Shokouhi^d, and Hossein Samadi Kafil ^{**b}

^a Department of Organic and Biochemistry, Faculty of Chemistry, University of Tabriz, Tabriz 5166614766, Iran.

^b Drug Applied Research Center, Tabriz University of Medical Sciences, Tabriz, Iran.

^c Chemical Injuries Research Center, Systems biology and poisonings institute, Baqiyatallah University of Medical Sciences, Tehran, Iran.

^d Connective Tissue Diseases Research Center, Tabriz University of Medical Sciences, Tabriz, Iran

^e Faculty of Chemistry, Department of Inorganic Chemistry, University of Tabriz, Tabriz, Iran

^f Infectious and Tropical Diseases Research Center, Tabriz University of Medical Sciences, Tabriz, Iran

Corresponding Authors:

* Ramin Karimian (karimian.r@gmail.com)

** Hossein Samadi Kafil (kafilhs@tbzmed.ac.ir)

Abstract

Nanotechnology has recently emerged as a promising field in biomedical applications especially in the targeted delivery of drugs to tumors. Besides, combination chemotherapy is common in cancer treatment and rapidly evolving. Therefore, the successfully delivery of chemotherapeutic drugs to the targeted cancer is a big challenge. In this study, we are endeavouring to develop a nano-vehicle, based on highly branched amine-functionalized p-sulfonatocalix[4]arene as a dual-drugs carrier for co-delivery of DOX and MTX to the MCF7 breast cancer cells with targeting and synergistic effects. After the synthesis and preparation of the nano-vehicle, its structural characterizations were also taken (FTIR, AFM, VSM, SEM, EDX, XRD, DLS, zeta potential analysis). Drug loading and release studies of prepared drugs-loaded nano-vehicle were studied to optimize the formulation. The designed platform has targeting and pH-triggered drug release capabilities to improve the therapeutic index of DOX and MTX. Hemolysis assay results were proved that the nano-vehicle has high blood compatibility even at the high dosage treatment. Protein-particle interaction of nano-vehicle in human blood circulation systems via SDS-PAGE assay was simulated and the results indicated that a series of proteins were attached to the surface of nano-vehicle. This feature gives stealth property to the nano-vehicle in blood circulation system. The cellular uptake by flow-cytometry and fluorescent microscopy were validated that the human plasma proteins attached to the nano-vehicle surface cause high internalization capability into the cells due to the presence of some protein receptors on the surface of cancer cells which improve the tumor cell targeting property. MTT assay and DAPI staining were also performed to show viability and DNA fragmentation of treated cells. All results validated each other and confirmed that our designed nano-vehicle is useful for targeted and combination drug delivery systems with stealth property.

Keywords: Combination chemotherapy, highly branched p-sulfonatocalix[4]arene , drug delivery, synergistic effect, stealth nano-vehicle.

1. Introduction

CANCER is the leading cause of death all over the world.¹⁻³ Cancer is a bio-complex disease with various factors and involving extensive phenotypic and genetic variations.⁴⁻⁶ Several approaches were developed for cancer treatment including surgery, chemotherapy, radiation therapy, hormone therapy, stem cell transplantation, and targeted therapy.⁷⁻¹⁰ Among the above mentioned items, chemotherapy is a conventional method for many kind of cancerous patients in clinical trials, but continuous administration of this method cause drug resistance.¹¹ To overcome the drug resistance, anticancer drugs were used with high doses which cause adverse side effects on other healthy organs.¹² Using single chemotherapeutic agents with these limitations could be improved by combination of two or more agents. Combination chemotherapy can kill cancer cells at lower dosages by affecting multiple anticancer drugs with synergistic effects and different mechanisms of action.^{13, 14} It has been proved that an appropriate combination of chemotherapeutic agents can improve the therapeutic effect because of using reduced dosage of chemotherapeutic agents and decreasing the drug resistance development.^{15, 16} However, finding an appropriate and applicable nano-vehicle is an important subject in co-delivery of drug agents and combination therapies.

Many types of nano-vehicles have been developed for drug delivery systems such as liposomal, polymeric, dendritic, metallic and carbon-based materials.¹⁷⁻²¹ Among these materials, nano-vehicles with dendritic architecture have specific topological structure with high capacity for conjugation by a variety of agents including chemotherapeutic drugs, genes, antibiotics and other biological agents in biomedical applications.²²⁻²⁴ Also, the presence of many repeating functional groups on the surface of the dendritic materials could improve their physicochemical properties.

Various kind of chemotherapeutic agents are used for cancer patients in clinical treatment. Cisplatin, Fluorouracil, Doxorubicin, Methotrexate, Docetaxel, Mercaptopurine, and etc. are anticancer drugs which are used commonly in medical applications. Doxorubicin (DOX) is a chemotherapeutic agent (anthracycline) and used for the various type of cancer.²⁵ Other anticancer drugs with different mechanism of action and synergistic effects are also use in combination with DOX.^{15, 24, 26, 27} Methotrexate (MTX) is an anticancer drug and also commonly used for treatment of many solid tumours.²⁸ As structural similarity of the MTX to folic acid (FA), MTX could act as a ligand to attach the folic acid receptor on the surface of the cancer cells such as MCF7 cells and enter cells through like FA transport system.^{29, 30}

Herein, we wish to report the developing a nano-vehicle based on dendritic p-sulfonatocalix[4]arene with highly branched amine-functionalized carrying two chemotherapeutic agents aiming to improve the drug loading efficiency and reducing side effects for combinational chemotherapies. The prepared nano-vehicle consisting of a hydrophobic calix[4]arene core and four arms of polyamidoamine chains that have been found to exert an excellent biocompatibility, stealth property, being devoid of intrinsic cytotoxicity, and has low hemolytic potential with good loading and encapsulation efficiency in compared to the other designed nanocarrier which are used in combination drug delivery systems.

2. Experimental sections

2.1. Materials

Calix[4]arene was synthesized according to Gutsche etal protocol.³¹ Chemical reagents including formaldehyde, phenol, aluminum chloride, sodium carbonate (Na_2CO_3),

epichlorohydrin, and ammonia solution (NH_4OH) were purchased from Merck Co. All solvents used in this study were also obtained from Merck Co. and used as received. Methyl acrylate (MA), ethylenediamine (EDA), Ferric chloride hexahydrate ($\text{FeCl}_3 \cdot 6\text{H}_2\text{O}$), ferrous chloride tetrahydrate ($\text{FeCl}_2 \cdot 4\text{H}_2\text{O}$), and 3-(4,5-dimethylthiazol-2-yl)-2,5-diphenyltetrazolium bromide (MTT) were purchased from Sigma-Aldrich Co. Doxorubicin (DOX) salt was obtained from Sobhan Pharmaceuticals Co. (Tehran, Iran) and Methotrexate (MTX) was kindly received from Zahravi Pharmaceuticals Co. (Tabriz, Iran). Human red blood cells (HRBCs) were kindly obtained from Iranian Blood Transfusion Institute which stabilized with ethylenediaminetetraacetic acid (EDTA). Deionized water was prepared by Milli-Q water system and used for all experiments. All materials using biological protocols, including trypsin, fetal bovine serum (FBS), and Roswell Park Memorial Institute 1640 growth medium (RPMI) were purchased from Gibco BRL Life Technologies. MCF7 cells as human breast cancer cells were purchased from Cell Bank, Pasteur Institute of Iran, Tehran, Iran.

2.2. Characterizations

2.2.1. FTIR: Fourier-transform infrared (FTIR) spectroscopy was used to monitor and analyze the formation of samples composition. FTIR spectra were recorded on a Bruker (Shimadzu, Japan) by KBr method. Sample discs were previously prepared with KBr at 1:50 (sample: KBr, w/w) and scanned against a blank KBr disk at wavenumbers ranging from 500 to 4000 cm^{-1} .

2.2.2. SEM-EDX: The morphology, size, and elemental percentage analysis of samples were investigated using a scanning electron microscopy (FESEM-EDX; TESCAN 5001). Prior to examination, samples were mounted onto a metal stub using a carbon double-sided adhesive tape, and covered with a thin layer of gold, with the aid of a direct current sputter technique

(Emitechk 450X, England). Furthermore, to accurately assess modification process, elemental analysis by Energy Dispersive X-Ray analysis technique was employed.

2.2.3. TEM: The transmission electron microscopy (TEM) analysis was also used to determine the size and morphology of the samples by a CM120, Philips, Germany with operating at 200 kV. Before analysis, the suspension was ultrasonically dispersed using a probe-type ultrasonic generator (400 W) for 10 sec and the suspension was placed on a copper grid within 2 min.

2.2.4. AFM: Topographic images of the samples were taken by atomic force microscopy (AFM) measurements (JPK Instruments AG, Berlin, Germany) in non-contact tapping mode. Before testing, a dilute solution of a sample was prepared in deionized water. Then, two droplets of the sample solution were dropped on a clean coverslip and allowed to vaporize the solvent.

2.2.5. VSM: Magnetic measurements of samples were analyzed with the aid of a vibrating-sample magnetometer (VSM; AGFM, Kashan, Iran) to evaluate the magnetic properties of samples at room temperature.

2.2.6. DLS and ζ potential: The particle size distribution and surface charge of samples were determined using a dynamic laser-scattering technique (DLS; Zetasizer Nano ZS90; Malvern Instruments, Malvern, UK). An appropriate amount of samples were added to the PBS solution and diluted to achieve the required sample density for analysis. The zeta (ζ) potential values were also assessed by the same instrument.

2.2.7. XRD: Powder X-ray diffraction patterns of the samples were recorded on a Bruker AXS model D8 Advance Diffractometer using $\text{CuK}\alpha$ radiation ($\lambda=1.542\text{\AA}$), with the Bragg angle ranging from $2\theta=10-80^\circ$.

2.3. Sequence steps in the preparation of magnetic nano-vehicle (D-Calix/MNPs)

2.3.1. Synthesis of p-sulfonatocalix[4]arene (s-Calix)

Calix[4]arene (1.0 g, 2.4 mmol) was added to 10 mL concentrated H₂SO₄ and the solution was heated at 70 °C for 3h. The reaction progress was monitored by adding gradually an aliquot of reaction mixture into the deionized water. After completion reaction, no precipitate materials were detected in the mixture. Then, reaction mixture was allowed to cool and poured gradually into 10 mL deionized water. The solution was neutralized with Na₂CO₃ solution, and evaporated to dryness. The residue was precipitated several times from water to ethanol. Finally, p-sulfonatocalix[4]arene was dried at 50 °C for 24 h (Fig. 1A).³²

2.3.2. Grafting amine functional groups on the surface of s-Calix (N-Calix)

To graft amine functional groups on hydroxyl groups at the surface of s-Calix following procedure was done according to the recent literature with slight modification.³³ In the first step, s-Calix (1 g) was dissolved in NaOH solution (2 M) for 20 min and then reacted with epichlorohydrin at 60 °C for 4 h. The reaction mixture was precipitated in ethanol several times to remove unreacted epichlorohydrin. In the second step, the reaction mixture was heated with NaOH solution (50% w/v), NH₄OH (29.4%) with pH 12 at 60 °C for 2 h (Fig. 1B). Finally, amino functional groups grafted on the surface of s-Calix (N-Calix) were obtained.

2.3.3. Preparation of dendritic p-sulfonatocalix[4]arene (D-Calix)

Two main reactions (Michael addition and amidation reaction) were used to obtain dendritic architecture on the surface of p-sulfonatocalix[4]arene which were made of repetitively branched

subunits of amide and amine functionality (**Fig. 1B**). Michael addition was done using methyl acrylate to obtain half generations of D-Calix in each step (0.5th, 1.5th, and 2.5th). In the following Michael addition step, amidation of terminal methyl ester groups using EDA was done to achieve full generations. The Michael addition and amidation steps were described in detail as follow:

Step 1 (Michael addition): p-sulfonatocalix[4]arene (1 g) was dispersed in 20 mL methanol and 1 mL methyl acrylate. The mixture was stirred vigorously under an inert atmosphere at 50 °C. After 48 h, the reaction mixture was precipitated in ethanol and centrifuged. The obtained precipitate (0.5th generation of D-Calix) washed repeatedly with ethanol several times to remove unreacted MA.

Step 2 (Amidation reaction): half generation of D-Calix was dispersed in 20 mL methanol and 1 mL EDA. The mixture was stirred vigorously under an inert atmosphere at 50 °C. After 48 h, the reaction mixture was precipitated in ethanol and centrifuged. The mixture was washed repeatedly with ethanol several times to remove unreacted EDA. Therefore, 1st generation of D-Calix was obtained dried in vacuum oven at 40 °C. The 2nd and 3rd generations of D-Calix were prepared by performing, Michael addition, and amidation reaction twice.

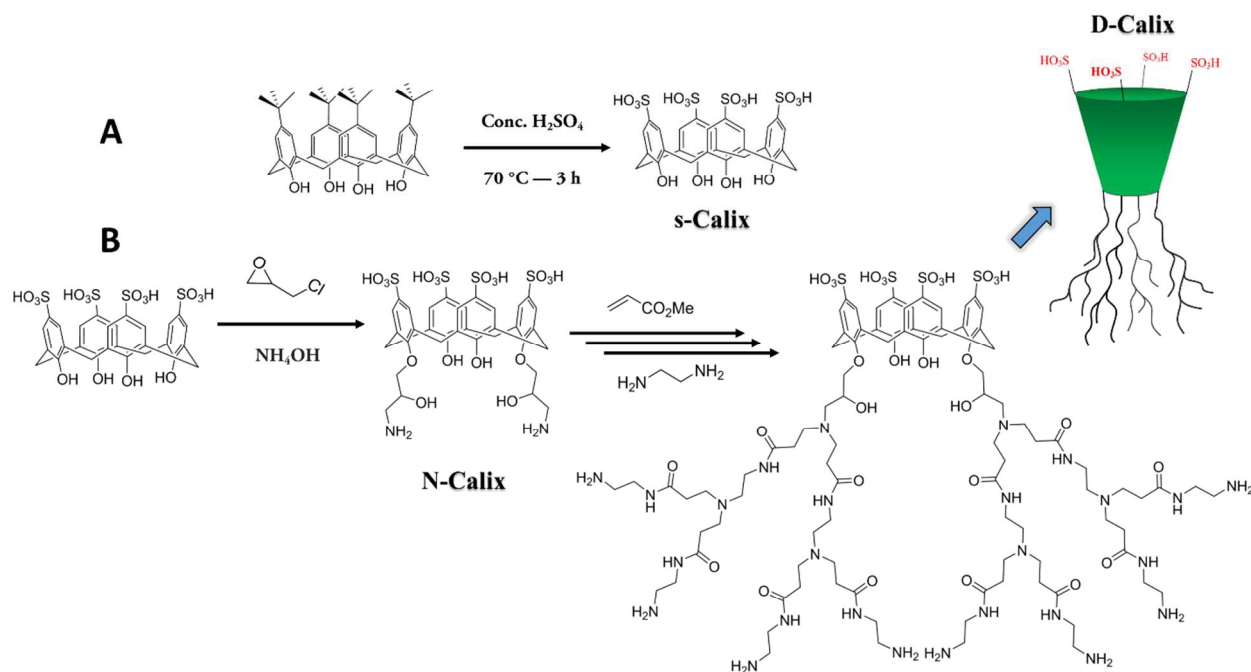


Figure 1: (A) Synthesis of p-sulfonatocalix[4]arene from calix[4]arene in concentrated sulfuric acid solution at $70\text{ }^\circ\text{C}$ for 3h. (B) Grafting amine functional groups on the surface of s-Calix to obtain N-Calix and preparation of D-Calix by performing Michael addition and amidation reactions

2.3.4. Preparation of dendritic p-sulfonatocalix[4]arene coated magnetic nanoparticles (D-Calix/MNPs)

To introduce D-Calix on the surface of MNPs following procedure was done. In brief, 0.5 g of Fe_3O_4 NPs was dispersed in 50 ml absolute methanol and 1 mL of [3-(2,3-epoxypropoxy)propyl]trimethoxysilane was added dropwise under stirring at room temperature. The reaction mixture was heated at $100\text{ }^\circ\text{C}$ for 6 h under nitrogen atmosphere. Subsequently, 0.5 g D-Calix was added to the reaction mixture and refluxed at $100\text{ }^\circ\text{C}$ for 24 h (**Fig. 2**). The D-Calix coated magnetic nanoparticles (D-Calix/MNPs) were collected with an external permanent magnet and washed several times with water/ethanol. For using D-Calix/MNPs as a magnetic

nano-vehicle in this study, the obtained NPs were dried under vacuum condition at 40 °C for 24 h.

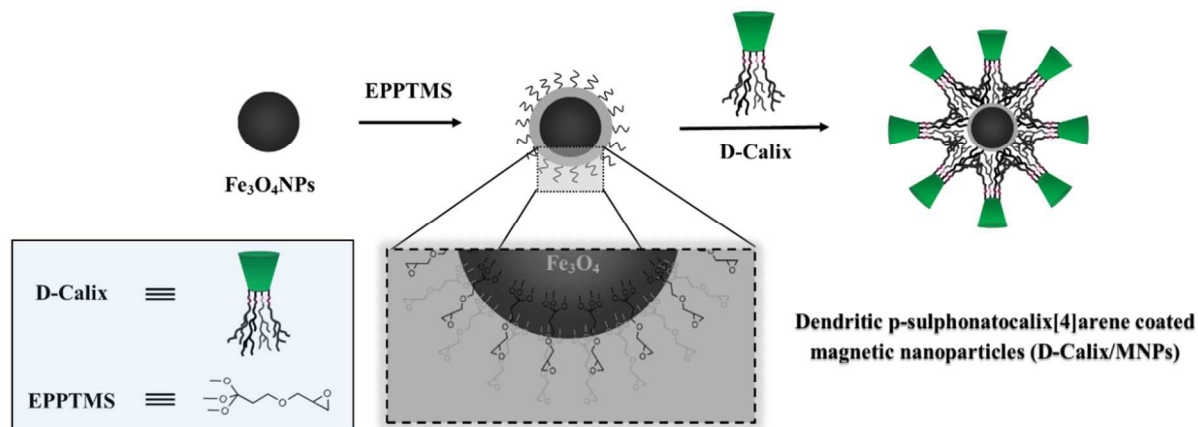


Figure 2: Surface modification of magnetic nanoparticles and preparation of dendritic p-sulphonatocalix[4]arene coated magnetic nanoparticles (D-Calix/MNPs)

2.4. Determination of amine functional groups grafting on the surface of D-Calix

Ninhydrin assay was performed to measure the formation of amine functional groups in the preparation of D-Calix.^{34, 35} Briefly, appropriate amount of s-Calix, N-Calix, D-Calix (1st, 2nd, and 3rd) and 2 mL of ninhydrin reagent (1% w/w) in PBS were mixed. The obtained mixture was heated in boiling water bath for 10 min. Afterward, the mixture was cooled to ambient temperature and diluted with 20 times with ethanol/water solution (1/1). The absorbance of each sample was scanned in the range of 400-800 nm against a blank reference by using a UV-visible spectrophotometer.

2.5. Preparation of protein corona on D-Calix/MNPs (Pro/D-Calix/MNPs) and protein-particle interaction evaluation by SDS-PAGE assay

Human plasma isolation: Human blood was obtained from Iranian Blood Transfusion Institute. The obtained blood was stabilized and centrifuged at 3000 rpm for 10 min. The upper layer (plasma) was collected and the pellets (red blood cells) were discarded. The isolated human plasma (HP) was kept in -20 °C for using in the following step.

Protein corona: 1 mL HP was diluted twenty times with PBS (pH 7.4) and appropriate amounts of nano-vehicle were dispersed in the container. The suspension was shaken and incubated at 37 °C for 2 h. The nano-vehicle was separated by an external permanent magnet and washed three times with PBS. Finally, the prepared Pro/D-Calix/MNPs (nano-vehicle/Pro) were used in the next step.

SDS-PAGE assay: Bounded proteins on the surface of nano-vehicle/Pro were released by using SDS-PAGE loading buffer. The released proteins in solution were loaded onto the 12% SDS-PAGE gel to separate the proteins. The SDS-PAGE gel was stained with 0.25% Coomassie brilliant blue R-250 solution after electrophoresis at room temperature for 4 h. Finally, the stained SDS-PAGE was taken in methanol and water solution and shaken by a shaker incubator. A photograph was taken from the gel by using a high-resolution scanner.

2.6. Hemolysis assay

Blood collection and erythrocyte isolation: Human bloods were obtained from Iranian Blood Transfusion Institute. An appropriate amount of whole blood which stabilized via EDTA was

taken and spun at 4000 rpm for 10 min at room temperature. The upper layer (plasma) was discarded and erythrocytes (red blood cells) were isolated. The isolated red blood cells (RBCs) were washed three times with PBS (pH 7.4) to obtain a clear supernatant.

Hemolytic activity and RBCs aggregation: A total isolated RBCs was diluted ten times by PBS (pH 7.4). In each well of 24-well plate, 0.5 mL different amount of nano-vehicle concentration (10, 50, 100, 200, 400, 800, 1600, and 3200 $\mu\text{g mL}^{-1}$) and 0.5 mL of diluted RBCs were mixed and incubated at 37 °C for 1h. After incubation, aggregations of RBCs were observed by phase contrast microscope (Nikon, YS2-T; Japan) with 40 \times magnification. Diluted RBCs which treated with 0.5 mL water and PBS used as the positive and negative controls with 100% and 0% hemolytic effects, respectively. At last, all samples were transferred to the microtubes and centrifuged at 5000 rpm for 5 min. The supernatant were taken out and transferred to the 96-well plate. The ELISA plate-reader was used to measure the released hemoglobin (at a wavelength of 540 nm) and calculate the hemolysis rate via following formula:³⁶

$$\text{Hemolysis Rate \%} = \frac{\text{Abs (Sample)} - \text{Abs (Positive Control)}}{\text{Abs (Positive Control)} - \text{Abs (Negative Control)}} \times 100$$

2.7. Drug loading and drug release in-vitro studies

Drug loading study: DOX and MTX were used as the model drugs for combination chemotherapy. Both chemotherapeutic agents were loaded into the drug carrier according to the following two steps. For DOX loading, 100 mg of nano-vehicle was dispersed in 2 mL PBS (pH 7.4) and 10 mg DOX was added to the suspension. The obtained suspension was stirred at a moderate rate by magnetic stirrer at room temperature in dark condition for 24 h. Finally, DOX/nano-vehicle was separated by an external permanent magnet and dried via vacuum oven

at room temperature. For MTX loading, 100 mg of DOX/nano-vehicle was dispersed in 2 mL PBS (pH 7.4) and 10 mg MTX was added to the suspension. The obtained suspension was stirred at room temperature in dark condition for 24 h. The resulting DOX/MTX/nano-vehicle was collected by an external magnet, and the supernatant was kept for the calculation of unloaded MTX and released DOX from the nano-vehicle. Finally, the collected precipitate as a DOX/MTX/nano-vehicle was dried and used for further *in-vitro* assays. To obtain DOX/nano-vehicle and MTX/nano-vehicle, all above procedure were also done alone.

Calculation of drug loading and encapsulation efficiency: Unbound DOX and MTX were calculated by measuring the characteristic absorption wavelengths of drugs with a UV-vis spectrophotometer. In brief, the supernatant from the above two steps was collected and the absorption wavelength was taken at 480 and 290 nm. The drug loading efficiency (DLE) and drug encapsulation efficiency (DEE) were calculated by the following formulas:

$$\text{DLE}(\%) = \frac{\text{Mass of drug in nano - vehicle (mg)}}{\text{Mass of nano - vehicle (mg)}} \times 100$$

$$\text{DEE}(\%) = \frac{\text{Mass of drug in nano - vehicle (mg)}}{\text{Mass of feed drug (mg)}} \times 100$$

In-vitro drug release study: After preparation of the drug-loaded nano-vehicle, 2 mL PBS solution (pH 7.4 and 5.0) as the release medium and 10 mg drug-loaded nano-vehicle were added into the microtube. The drug release study was performed at 37 °C and at different time intervals, 2 mL of medium was taken out and 2 mL of fresh medium was replaced. UV-vis spectrophotometer was used to measure the concentrations of released DOX and MTX at 480 and 290 nm, respectively. All experiments were done in triplicates, and average data was reported.

$$\text{DOX and MTX release (\%)} = \frac{\text{amount of DOX or MTX release (\mu g)}}{\text{amount of DOX or MTX on nano - vehicle (\mu g)}} \times 100$$

2.8. Cell Culture

MCF7 cells (human breast cancer cells) were obtained from Pasteur Institute of Iran, Tehran, Iran and maintained in RPMI 1640 medium supplemented with 10% FBS and 1% benzylpenicillin/streptomycin. The cells were incubated under a humidified atmosphere and 5% CO₂ at 37 °C for 24 h to attach to the bottom the flask. After reaching cells with 90% confluence, the cells were detached by adding trypsin to the flask. The cell suspensions were collected and centrifuged at 1500 rpm for 5 min and re-suspended in the growth medium for further steps.³⁷

2.9. Cytotoxicity studies

The MCF7 cells were seeded at a density of 5×10³ per well in 96-well plates. The cells were incubated for an overnight and treated with the free DOX, free MTX, DOX/MTX, and DOX/MTX/nano-vehicle at the concentration of 0.25, 0.50, 1.0, 2.00, 4.00, and 8.00 μg mL⁻¹ (single and dual drugs) for 48 h. The cells were also treated with blank nano-vehicle to show their biocompatibility at the same condition and concentration of 2.5, 5.0, 10.0, 20, 40, and 80 μg mL⁻¹. Afterward, the culture media was exchanged with 180 μL fresh culture media and 20 μL MTT solution (2 mg mL⁻¹) and incubated at 37 °C for 4 h. The MTT solution was removed and replaced with 200 μL dimethyl sulfoxide (DMSO) with 20 min incubation time. The optical density values of each well (dissolved formazan crystals) were measured at a wavelength of 570 nm using an ELISA reader.

2.10. Combination effect analysis

The Combination Index (CI) was calculated based on the Chou–Talalay method for study the DOX and MTX interaction.³⁸ The following formula was used for calculating the CI:

$$CI = \frac{AB}{A \times B}$$

CI was used to evaluate synergy effects of DOX and MTX combination against MCF7 cells *in-vitro*; where, AB is the cell viability of the combination group relative to the control group, and A and B are the cell viability of DOX and MTX relative to the control group which CI less than one, equal to one, and more than one indicate synergistic, additive, and antagonistic effects, respectively.

2.11. Targeted cellular uptake assay by fluorescence microscopy and flow-cytometry

Fluorescence microscopy: DOX has fluorescence and is used as a marker to measure the cellular uptake of nano-vehicle. DOX labelled nano-vehicle was prepared according to experimental section. The sterile coverslips were placed in the bottom of a six-well plate. Then, MCF7 cells were seeded at a density of 5×10^4 into the six-well plate and incubated for 24 h to growth. The seeded cells were treated with DOX labelled nano-vehicle and nano-vehicle/pro at a concentration of $50 \mu\text{g mL}^{-1}$ and incubated for 2 h. After incubation, the cells were washed three times with PBS and fixed by formaldehyde (4% w/v). The coverslip was taken onto a glass microscope slide and nano-vehicle uptake was observed by using a fluorescence microscope (Olympus microscope Bh2-RFCA, Japan).

Flow-cytometry: Quantitative cellular uptake of DOX labelled bare nano-vehicle and nano-vehicle/pro was also analyzed by using flow cytometry (Becton Dickinson Immunocytometry

Systems, San Jose, CA, USA).³⁹ In six-well plates, MCF7 cells were seeded at a concentration of 4×10^5 and incubated for a day to attach and grow at the bottom of each well. The cells were treated with DOX labelled nano-vehicle and nano-vehicle/pro at a concentration of $50 \mu\text{g mL}^{-1}$ and the cells with no treatment were considered as the negative control. After 2 h incubation, the cells were trypsinized and collected for determination of DOX uptake inside the cells via fluorescence intensity.

2.12. Apoptosis assay by DAPI staining

Apoptosis induction properties of the samples upon treatment of MCF7 cells were evaluated by microscopic analysis of DAPI staining. Briefly, 5×10^4 MCF7 cells were seeded in the six-well plates which have 12 mm sterile coverslips. The cells allowed attaching at the bottom of each well at 37°C for overnight. Then, the cells were treated with free MTX, free DOX, DOX/MTX, and DOX/MTX/nano-vehicle. The blank nano-vehicle was also used to show its cytocompatibility. The cells with no treatment were considered as negative control. After incubation for 48 h, the wells were washed three times with PBS and fixed with 4% formaldehyde at ambient temperature for 20 min. After washing the cells with PBS, cells were permeabilized by adding Triton X- 100 (0.1% w/v) and incubated for 5 min. Finally, the cells were washed again and stained by adding $300 \mu\text{L}$ of DAPI (200 ng/mL) on the coverslips for 20 min under dark condition. DNA condensation and fragmentation in apoptotic cells were evaluated under a fluorescence microscope (Olympus microscope Bh2-RFCA, Japan).

2.13. Statistical analysis

All data were reported as mean \pm SD of three replicates. The ANOVA or student's t-test were used for statistical analysis. The p-values less than 0.05 were considered significant.

3. Results and discussion

3.1. Preparation and characterization

In the present work, we are endeavoring to develop a biocompatible and pH-responsive magnetic nano-vehicle. The synthetic route for the preparation of nano-vehicle is given in **Fig. 1-2**. Firstly, the calix[4]arene and p-sulfonatocalix[4]arene were prepared according to the published procedures. In order to introduce amine functional groups on the hydroxyl side, p-sulfonatocalix[4]arene was reacted with epichlorohydrin and ammonia solution. Different generation of D-Calix was synthesized via performing two main reactions (Michael addition and amidation). D-Calix has internal molecular architecture consisting of tree-like branching which each generation has exponentially more branching points. In the end, magnetic nanoparticles were modified by obtained D-Calix with highly amount amine functional groups to produce final magnetic nano-vehicle. Both DOX and MTX as model anticancer drugs were loaded on the nano-vehicle and used in the further *in-vitro* evaluation of MCF7 breast cancer cells. After the synthesis and preparation of the nano-vehicle, its structural characterizations were also taken including FTIR, AFM, VSM, SEM, EDX, XRD, DLS, zeta potential analysis which discussed in the following:

Fig. 3 showed the FTIR spectra of Calix, s-Calix, N-Calix, and different generation of D-Calix (1st, 2nd, and 3rd). The Calix has three main C-O, C-H, and O-H bonds which were appeared at about 1205, 2954, and 3201 cm⁻¹, respectively. It has four tert-butyl substituents at the para position with many aliphatic C-H bonds which increased the intensity of peaks at about 2860 to 2954 cm⁻¹ (**Fig. 3a**). As the tert-butyl substituted of Calix was exchanged with sulfonate groups in s-Calix, the peaks related to the C-H stretching bonds at about 2850-2950 cm⁻¹ was significantly decreased and it was proved that substitution was done successfully. Besides, the characteristic peaks at 1045 cm⁻¹ were assigned to the sulfonate functional groups (-SO₃) (**Fig. 3b**). In the third step, the hydroxyl groups on s-Calix were reacted with epichlorohydrine and ammonia to introduce amine functional groups. As seen in **Fig 3c.**, the characteristic bonds of -SO₃, C-H, O-H, and N-H in N-Calix were appeared at 1045, 1122, 3361, and 3403 cm⁻¹ in FTIR spectra, respectively. The hydroxyl and amine stretching vibration bonds were overlapped, therefore, the peak intensity was enhanced which confirm the formation of both functional groups. The peaks of C-H stretching vibration bond were also increased due to the formation of -CH₂- bonds. By growing the dendritic architecture on the surface of N-Calix via performing two main reactions (Michael addition and amidation reaction), ester and amine functional groups were shown in D-Calix-G₃ at about 1704 and 3500 cm⁻¹, respectively. Furthermore, the bands attributed to the C-H bonds at about 2920 cm⁻¹ were also enhanced due to the formation of several -CH₂- bonds (**Fig. 3d**). The synthesis of Fe₃O₄ NPs, as well as D-Calix/MNPs, was confirmed by FTIR spectral analysis. In the FTIR spectrum of Fe₃O₄ NPs, the peaks at 563 cm⁻¹ related to the stretching vibration bond of Fe-O bonds (**Fig. 3e**). The appearance of bands at 1074 and 817 cm⁻¹ as illustrated in **Fig. 3f**, are corresponded to the symmetric and asymmetric stretching vibration of framework and terminal Si-O- groups. On the other hand, the appearance

of C-H, C-O, and C-C stretching vibration bonds at 2908, 1093, and 960 cm^{-1} with weak intensities are attributed to the formation of D-Calix/MNPs.

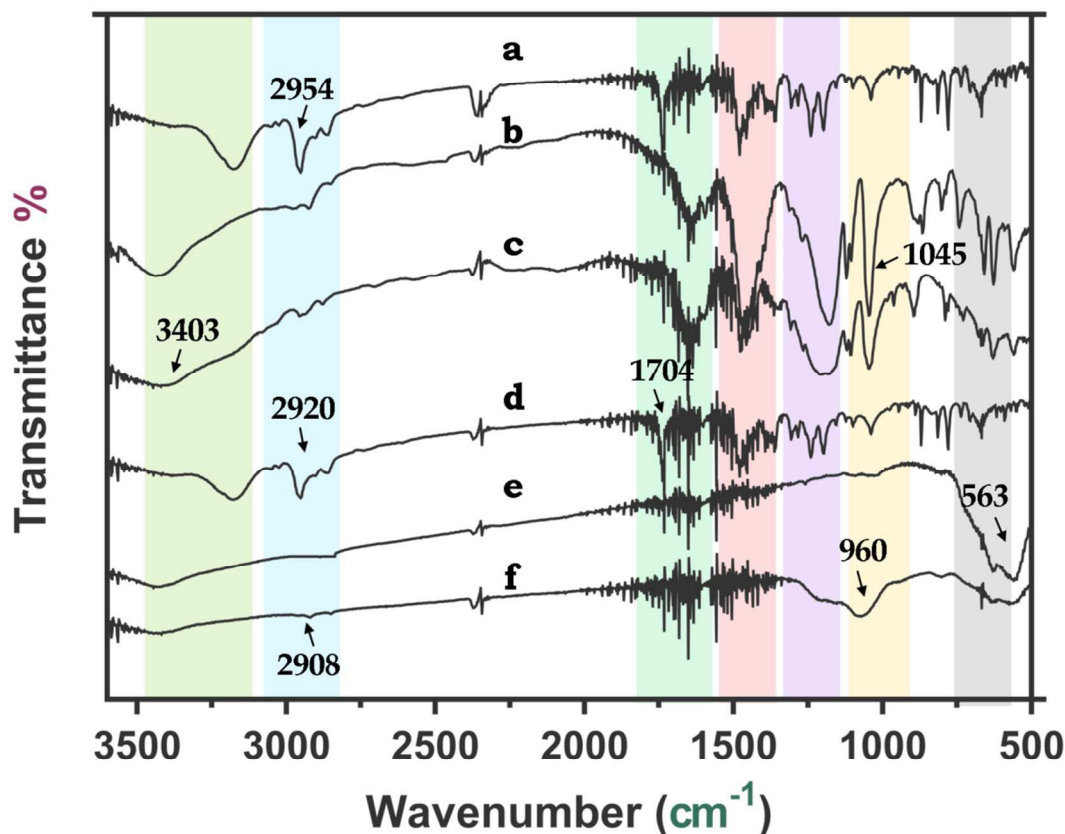


Figure 3: FTIR spectra of Calix (a), s-Calix (b), N-Calix (c), D-Calix-G₃ (d), Fe₃O₄ NPs (e), and D-Calix/MNPs (f). All samples were recorded with KBr disc at wavenumbers ranging 500-4000 cm^{-1}

SEM is a commonly used technique to study the size, morphology and elemental analysis of nanoparticles. SEM images of Fe₃O₄ and D-Calix/MNPs were shown in **Fig. 4A**. By observing the SEM graph of pure Fe₃O₄, it can be seen that the nanoparticles are well aggregated due to the nano-size of nanoparticles at about 10 nm. In the case of D-Calix/MNPs, a continuous SiO₂ layer was clearly coated on the outer surface of the Fe₃O₄ core which still maintained their spherical

shape after the coating process. The SEM image of D-Calix/MNPs has rough surface in compared to the Fe_3O_4 nanoparticles which indicate that the D-Calix as a dendritic macrocycle were grafted successfully onto the surface of nanoparticles. After careful evaluation of the SEM image, it was found that the aggregation of the nanoparticles were decreased which could help the final nano-vehicle for its stability. The observed aggregation which is seen in the SEM graph is related to the sample preparation. To confirm our claim we further analyzed the sample with TEM technique.

Therefore, to observe and determine the morphology and shape of final nano-vehicle, TEM analysis was applied. As seen in **Fig. 4B**, the nano-vehicle has nearly spherical shape and with dark core in some nanoparticles attributed to the magnetic core. To indicate shape and structure of prepared nano-vehicle clearly, TEM image was enlarged which exhibits low aggregation and semi-spherical shape with size of under 15 nm.

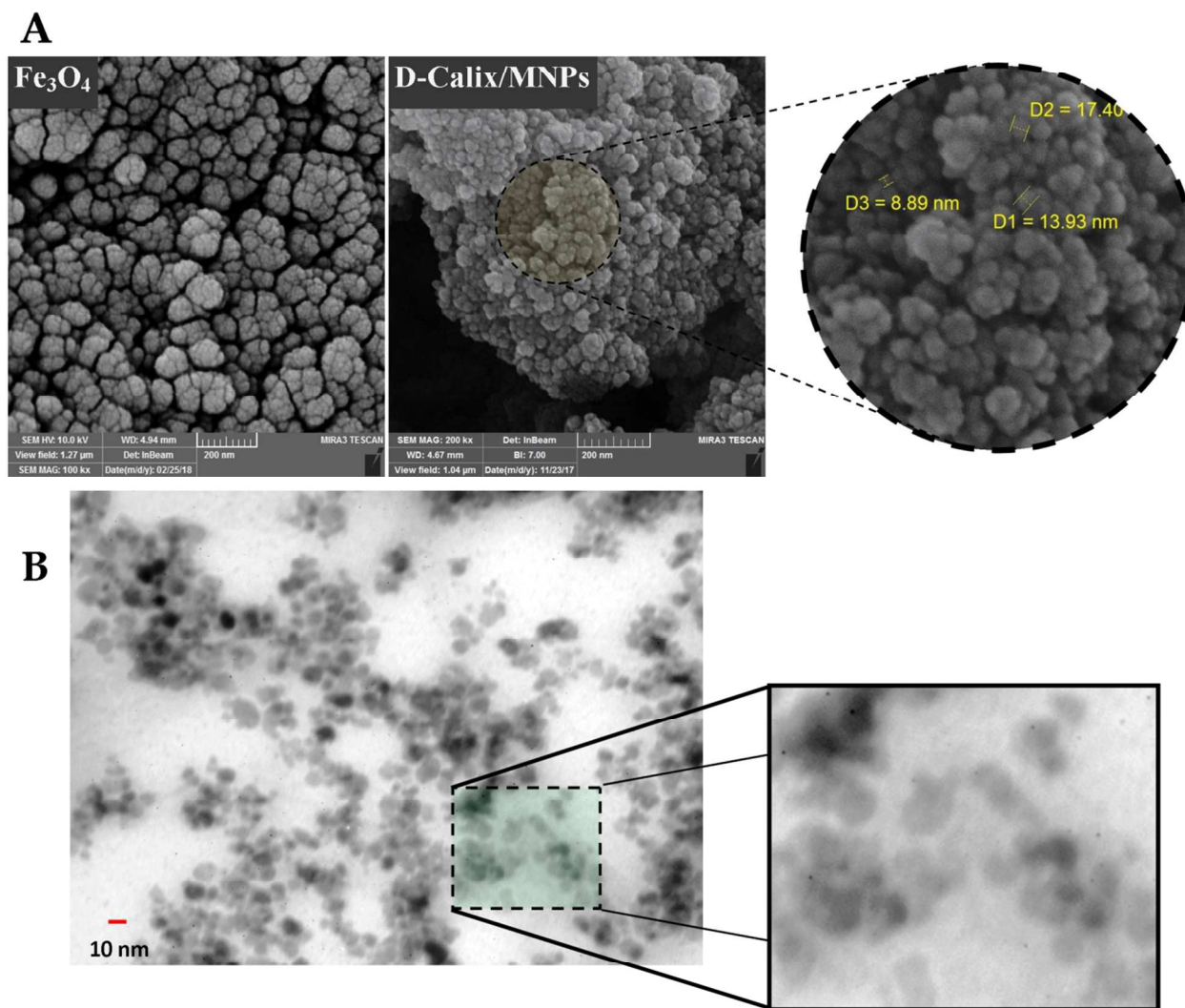


Figure 4: (A) SEM images of pure Fe_3O_4 NPs and D-Calix/MNPs for size and surface morphology studies. Both pure Fe_3O_4 and D-Calix/MNPs have relatively spherical shape with smooth and rough surface, respectively. (B) TEM images of magnetic nano-vehicle with spherical shape and low aggregation

The presence of elements (Carbon; C, Oxygen; O, Nitrogen; N, Iron; Fe, and Silicon; Si) and EDS analysis data with weight and atomic percentages were determined semi-quantitatively selected area energy dispersion spectrum (EDS) which summarized in **Table 1**. However, EDS is

a quantitative analysis for heavy element and in the case of light elements, EDS couldn't give the precise result. The results may vary in composition at different scan point, therefore, EDS analysis was done for each sample in triplicate. Fe_3O_4 NPs was used as a standard comprising Fe and O elements with the atomic weight percentage of $84.17 \pm 6.81\%$ and $39.64 \pm 4.97\%$, respectively. To verify the successful surface modification of Fe_3O_4 NPs with silica (SiO_2) layer and D-Calix, EDS analysis data with weight percentage was also done for D-Calix/MNPs and compared with pure Fe_3O_4 NPs. By observing the data in **Table 1**, the weight percentage of D-Calix/MNPs was 35.60 ± 5.13 , 43.21 ± 8.32 , 4.23 ± 0.92 , 14.41 ± 4.44 , and 2.55 ± 0.61 for Fe, O, Si, C, and N, respectively. Grafting D-Calix on the surface of Fe_3O_4 NPs caused the atomic weight ratio decreasing of Fe and O atoms. On the other hand, increasing the atomic percentage of C, N, and Si was validated that immobilization and grafting of D-Calix were successful (**Fig. 5**).

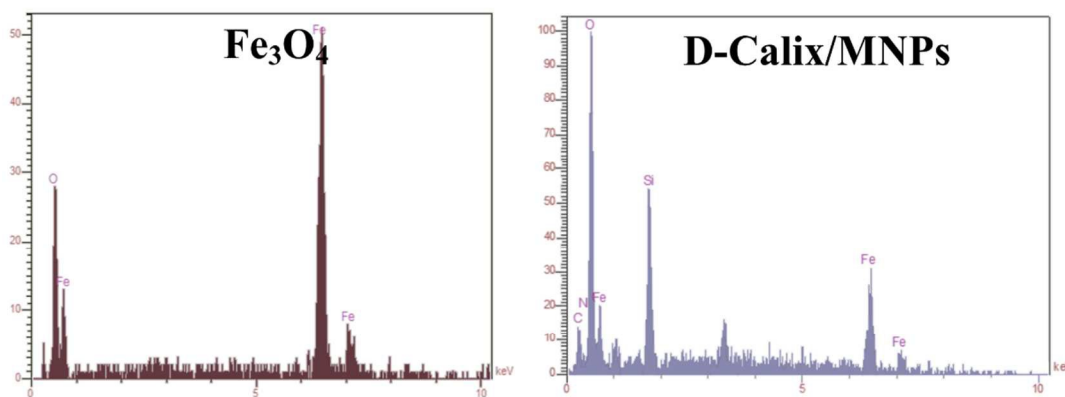


Figure 5: EDX analysis graph of pure Fe_3O_4 NPs and D-Calix/MNPs

Table 1: EDX quantification element normalized data of the pure Fe₃O₄ NPs and D-Calix/MNPs with weight and atomic percentage

Elm.	Fe ₃ O ₄		D-Calix/MNPs	
	W% ^a	A% ^b	W%	A%
Fe	84.17 ± 6.81	39.64 ± 4.90	35.60 ± 5.13	17.24 ± 4.62
O	15.83 ± 3.20	60.36 ± 7.45	43.21 ± 8.32	52.28 ± 11.45
Si	-	-	4.23 ± 0.92	3.15 ± 0.87
C	-	-	14.41 ± 4.44	23.91 ± 5.70
N	-	-	2.55 ± 0.61	3.42 ± 0.45
Total	100.00	100.00	100.00	100.00

^a W% = Weight percentage ^b A% = Atomic percentage.

To show the topological structure and unique properties of branched materials, atomic force microscopy (AFM) was used for analyzing the surface topography. The topological morphology of material surface has an important impact on their properties. The structure of dendritic materials has several advantages including the higher concentration of functional terminal groups and larger architectural constraints. As D-Calix was prepared by introducing the proper reactive groups onto the surface via a variety of chemical reactions, interesting and special morphologies was observed (**Fig. 6**). Due to the presence of tree-like branching on the side of the D-Calix, the AFM image showed uneven surface. These interesting features made the highly branched D-Calix suitable candidate as a drug nano-vehicle.

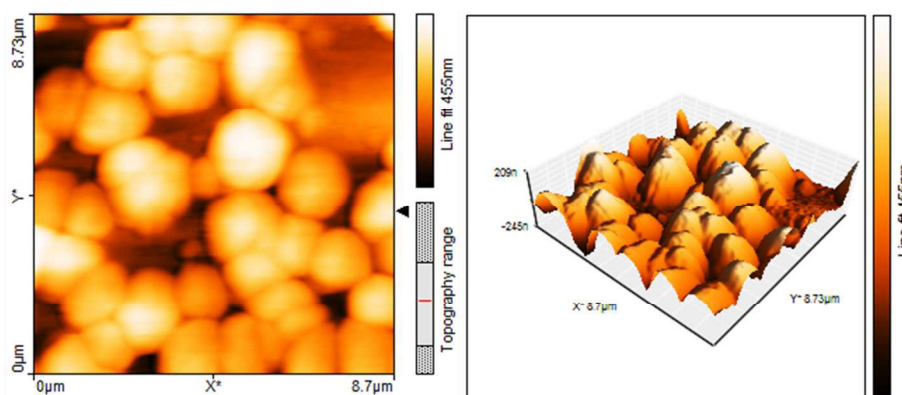


Figure 6: Surface topography of D-Calix by AFM analysis. D-Calix with uneven surface due to the presence of tree-like branching

For determination of particle size distribution of prepared nano-vehicle, a dynamic light scattering (DLS) technique was used and illustrated as a graph in **Fig. 7**. The average hydrodynamic particle size of nano-vehicle is reported around 100 nm in contrast to the SEM. In DLS technique, the hydrodynamic diameter was determined, while SEM technique measured the diameter of dried samples. The surface charge of nano-vehicle in PBS solution at pH 7.4 (zeta potential value) was measured and reported -2.5 mV. The presence of many amino functional groups (-NH₂) on the surface of D-Calix and presence of hydroxyl (-OH) and sulfonate groups (-SO₃H) on the other side of D-Calix cause an overall negative value for final nano-vehicle.

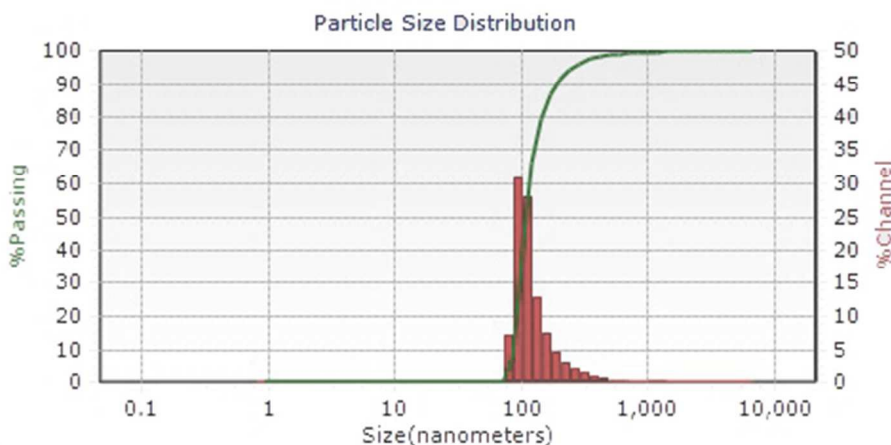


Figure 7: Particle size distribution of prepared nano-vehicle by DLS technique

Typical magnetization curve of blank Fe₃O₄ (MNPs) and prepared D-Calix/MNPs as a magnetic nano-vehicle was shown in **Fig. 8**. As seen in the magnetization curve, the remanent magnetization (remanence) and magnetic coercivity (coercive force) are about zero which has shown no magnetic hysteresis loops, indicating the characteristic superparamagnetic behavior of

MNPs and nano-vehicle.⁴⁰ The saturation magnetization of MNPs and D-Calix/MNPs are approximately 75 and 65 emu g⁻¹, respectively. The decreasing saturation magnetization value of D-Calix/MNPs is attributed to the existence of a thin layer of silica and D-Calix around MNPs. The high magnetic response of prepared D-Calix/MNPs (nano-vehicle) is also seen by applying an external permanent magnet with collecting beside the container in less than 30 seconds. After one week, the suspension was dried in vacuum oven at room temperature and the saturation magnetization of the nano-vehicle was measured for comparison with the original one. The slightly decreasing in saturation magnetization and the observed results are confirmed that D-Calix/MNPs has appropriate magnetic properties for biomedical applications and drug delivery systems.

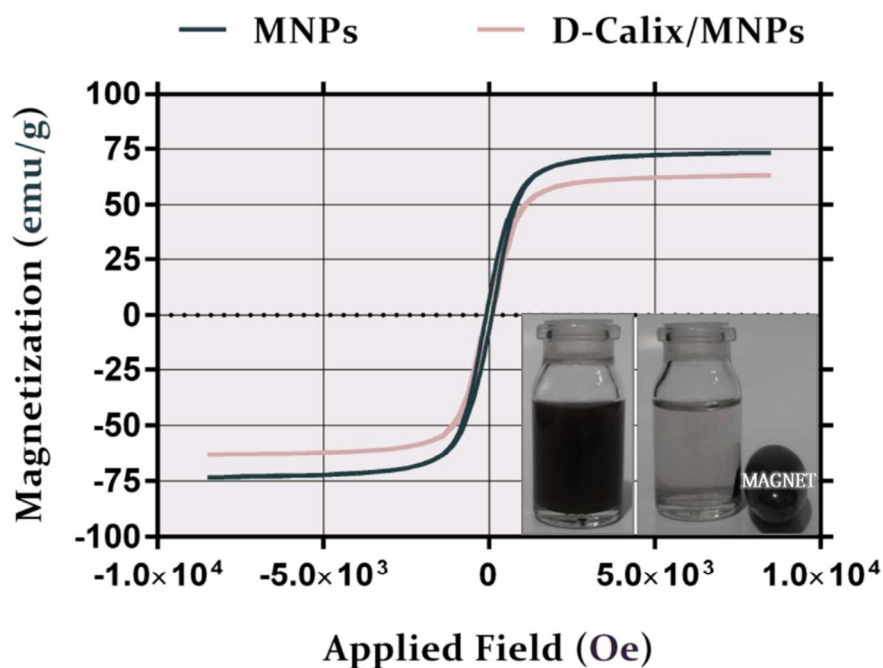


Figure 8: Magnetic properties of MNPs and D-Calix/MNPs with 75 and 65 emu g⁻¹ values, respectively. This value is appropriate for biomedical applications

The XRD patterns of the bare Fe₃O₄ and D-Calix/MNPs as a nano-vehicle were presented in **Fig. 9**. A series of characteristic peaks for Fe₃O₄ was appeared in the both samples which assigned in the graphs. These peaks are consistent with the standard pattern for Fe₃O₄ (JCPDS #19-629) with a cubic inverse spinel structure. The results indicated that the silica coating and grafting of D-Calix with whole preparation processes did not change significantly the crystal structure and phase change of the Fe₃O₄ nanoparticles. The average crystallite size D is calculated using the Debye–Sherrer equation, $D = K\lambda/(\beta\cos \theta)$, where K is a constant (K= 0.9 for Cu-K α), λ is wavelength (0.15405 nm for Cu-K α), β is the peak width of half-maximum and θ is the diffraction angle.

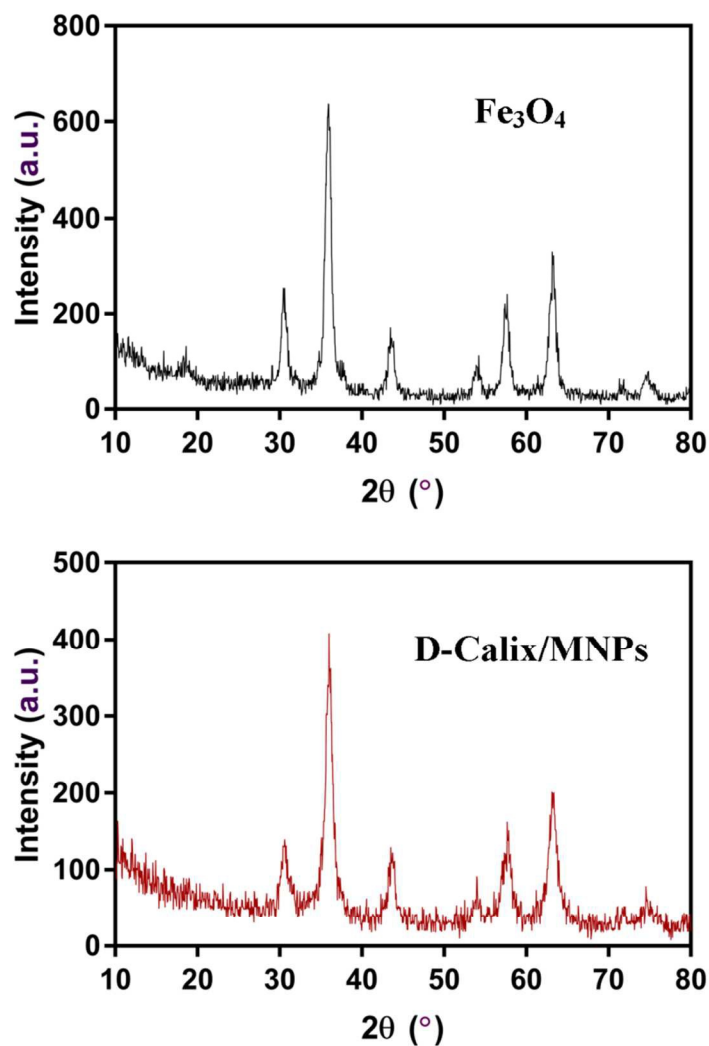


Figure 9: XRD pattern of Fe_3O_4 and D-Calix/MNPs

3.2. Quantification of amine functional groups on the surface of s-Calix, N-Calix, and D-Calix (G1, G2, G3)

To confirm the successfully grafting amine functional groups on s-Calix could be readily assessed by the ninhydrin assay. Ninhydrin reagent can react with primary and secondary amines via oxidative-reductive reaction resulting Ruhemann's purple color with a maximum absorbance

at 570 nm. The purple color intensity (Ruhemann) is proportional to the amine functional groups number. As seen in **Fig. 10**, s-Calix couldn't change the ninhydrin solution color because it has no primary and secondary amine functional groups and the absorbance graph has no peak at the range of 400-800 nm. Ninhydrin reagent was also reacted with N-Calix and the color of the mixture was changed to purple which confirmed the presence of amine moieties. By increasing the generation of D-Calix, the purple color intensity was also increased and it was confirmed our modification process. The absorbance graph of D-Calix-G₂ and D-Calix-G₃ has no significant difference and it was concluded that modification couldn't perform well after 2nd generation due to the highly steric hindrance.

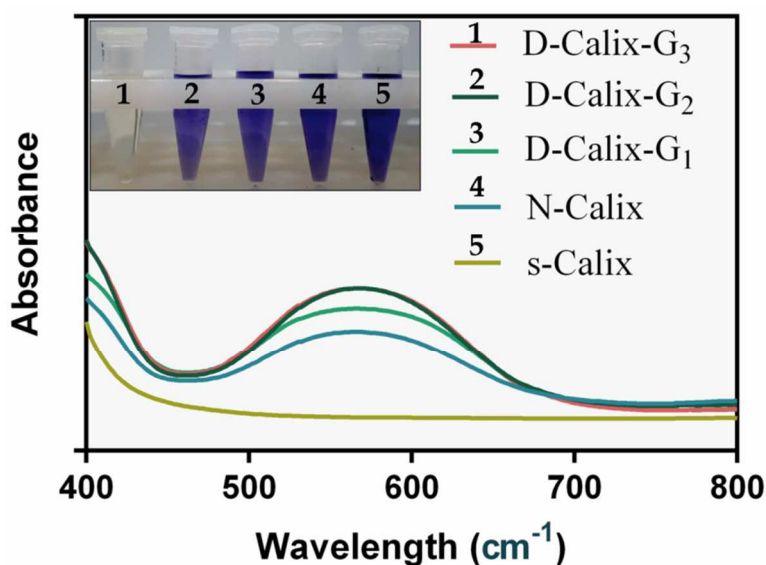


Figure 10: Ninhydrin assay for determination of amine functional groups. The graph was depicted based on absorbance versus wavelength

3.3. Stability of the nano-vehicle in PBS solution (human blood condition)

Bare MNPs is highly unstable in aqueous solution because of their tendency to aggregation and sedimentation. To improve the un-stability, MNPs surface was modified with some materials and the stability significantly enhanced. To evaluate the stability of our nano-vehicle in this report, the appropriate amount of D-Calix/MNPs was put in a vial with PBS solution (pH 7.4) and dispersed under probe sonicator for 5 min. The suspension was stored for several days and its behavior and stability were investigated. It was found that the suspension has no significant macroscopic changes and stability. All above results were confirmed that the magnetic nano-vehicle could easily inject into blood vessels without any aggregation and sedimentation.

Usually bare Fe_3O_4 starts to leach out in pH lower than 5.0. To investigate the Fe-leaching into solution, the final magnetic nano-vehicle was dispersed in PBS solution (pH 5.0) and incubated at 37 C for 24 h. The nano-vehicle was collected with an external magnet the supernatant was taken out to measuring Fe-leaching to the medium. The results were shown that leaching of the Fe was negligible. It was concluded that the silica layer with D-Calix coating could prevent Fe-leaching to the medium.

3.4. Biocompatibility of nano-vehicle on human red blood cells

The FDA recommends that materials intended for injectable use, an *in-vitro* hemolysis study should be performed at the intended concentration for intravenous administration to test for hemolytic potential.⁴¹ In this regard, the hemolysis assay was used to evaluate the cytotoxic effect of nano-vehicle on human RBCs due to the dendritic materials have been known to cause membrane damage to RBCs.⁴² According to the protocol in the experimental section, the RBCs were exposed to nano-vehicle at the range of concentrations from 10 to 3200 $\mu\text{g mL}^{-1}$ for 2 h (various model dosages which is used for *in-vivo* experiments). As seen in **Fig. 11**, the dose-

dependent hemolytic effect of nano-vehicle on RBCs was observed and the results were confirmed that there are only little hemolytic effects of nano-vehicle at high dosage. RBCs were also treated with nano-vehicle at a moderate concentration dosage ($200 \mu\text{g mL}^{-1}$), PBS, and deionized water. By observing the RBCs under phase contrast microscope, there is only low aggregation and changes (**Fig. 12**); whereas, PBS and water as the negative and positive controls have diskocytes and lysis form, respectively. It was found that nano-vehicle in this study has shown concentration-dependent hemolytic effect with lower than the permissible range which would make it suitable for the intravenous injection and *in-vivo* application.

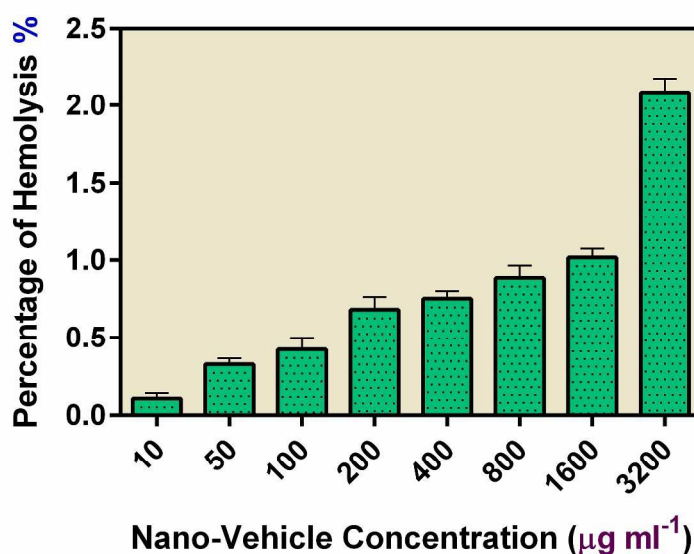


Figure 11: Hemolysis rate of HRBCs in the presence of nano-vehicle at different concentrations

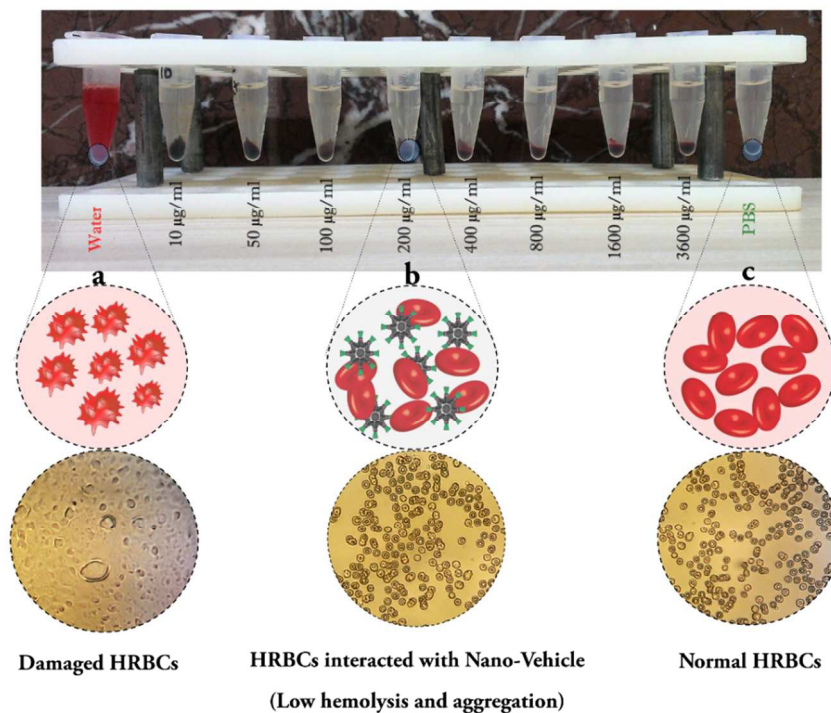


Figure 12: Visual observation of the presence of hemoglobin in the supernatant and optical images of HRBCs under phase contrast microscope after treatment with water (a), nano-vehicle with a concentration of $200 \mu\text{g mL}^{-1}$ (b), and PBS (c)

3.5. SDS-PAGE assay

For drug delivery applications, nanomaterials are commonly used intravenously to reach the target tumor cells. Average two thousand proteins exist in the human plasma which could decorate the surface of nanoparticles and resulting protein corona. Several proteins in human plasma such as transferrin (80 kDa), vitronectin (75 kDa), and apolipoprotein AI (28 kDa) have receptors on the surface of the breast cancer cells.⁴³ Besides, nanoparticles with these plasma proteins may influence uptake and potentially affect distribution and delivery to the intended target sites.⁴⁴ Therefore, we have employed a comprehensive approach to determine the human plasma proteins which have decorated the nano-vehicle. In this regards, D-Calix/MNPs as a

nano-vehicle was incubated with human plasma to mimic a simulated physiological blood stream condition after intravenous injection and qualitatively determined the proteins which available on the surface the nano-vehicle. For identification of bounded proteins to the nano-vehicle, the SDS-PAGE assay was performed according to Rahimi et al. previous article.⁴⁵ As seen in **Fig. 13**, several proteins were attached to the nano-vehicle surface which all protein bands in SDS-PAGE (12%) remain after 3 times washing (lane 2). Human plasma was used as an experimental control (lane 1) to know which proteins were bounded to the nano-vehicle after incubation for 1 h. Proteins ladder is used in lane 3 in order of decreasing molecular weight ranging from 10-245 kDa as a control. By bounding plasma proteins on the surface of nano-vehicle, most of their toxic effects were decreased due to their low reactivity with cellular membrane and perturbing plasma membrane. Therefore, masking nano-vehicle surface with proteins could be improved the biocompatibility.

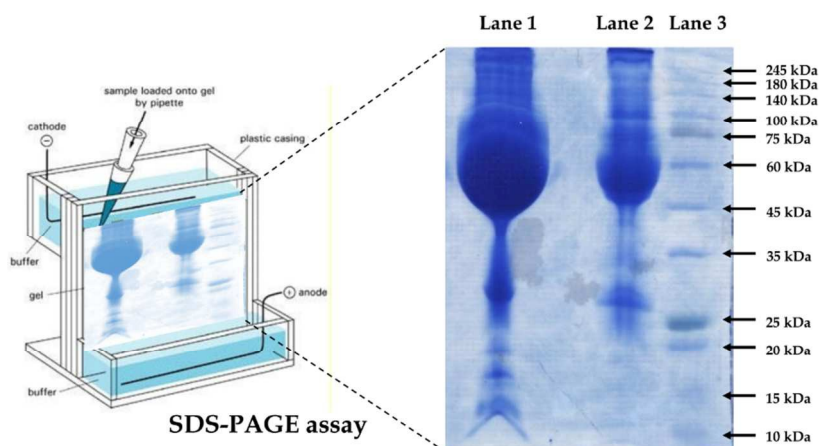


Figure 13: SDS–PAGE analysis. Bounded protein bands after three washing steps of nano-vehicle protein complex (lane 2), all protein bands of human plasma after dilution 20 times (lane 1), and protein ladder ranging from 10-245 kDa (lane 3)

3.6. *In-vitro* loading and release studies

Loading and releasing both DOX and MTX drugs of DOX/nano-vehicle, MTX/nano-vehicle, and DOX/MTX/nano-vehicle were examined for using further *in-vitro* experiments and the amounts of DOX and MTX content were determined by the visible spectrophotometric method. The drug loading efficiency of DOX/MTX/nano-vehicle for DOX and MTX was 6.32 ± 0.21 and 5.87 ± 0.77 , respectively. The drug loading efficiency of DOX/nano-vehicle and MTX/nano-vehicle was also reported 8.10 ± 0.45 and 6.98 ± 0.53 for DOX and MTX, respectively. Furthermore, the drug encapsulation efficiency for DOX and MTX was calculated for DOX/MTX/nano-vehicle 63.28 ± 2.89 and 58.74 ± 3.64 . The drug encapsulation efficiency of DOX/nano-vehicle and MTX/nano-vehicle was also obtained 81.02 ± 4.53 and 69.82 ± 5.36 for DOX and MTX, respectively. The release profiles of DOX and MTX were illustrated in **Fig. 14**. The release studies were investigated for about 300 h (about 12 days) which have shown a burst and rapid release at the beginning of the study for both DOX and MTX. These are attributed to the drugs which attached to the surface of the nano-vehicle. After investigation of about 300 h release study of DOX/MTX/nano-vehicle, 80.73 ± 2.03 and 87.53 ± 2.13 of total encapsulated drugs were released for DOX and MTX, respectively. The release studies of DOX/nano-vehicle and MTX/nano-vehicle were also evaluated and their graphs were illustrated as below. The results were shown that the overall DOX and MTX release in single drug loaded form were higher than dual drugs loaded from which are 92 ± 1.50 for DOX and 95 ± 0.78 for MTX at pH 5.0. In the same release condition, MTX has faster drug release than DOX and it might afford to the high hydrogen bonding of DOX with the nano-vehicle and another reason for the high total release of MTX is for its low encapsulation efficiency in compared to DOX.

DOX/MTX/nano-vehicle

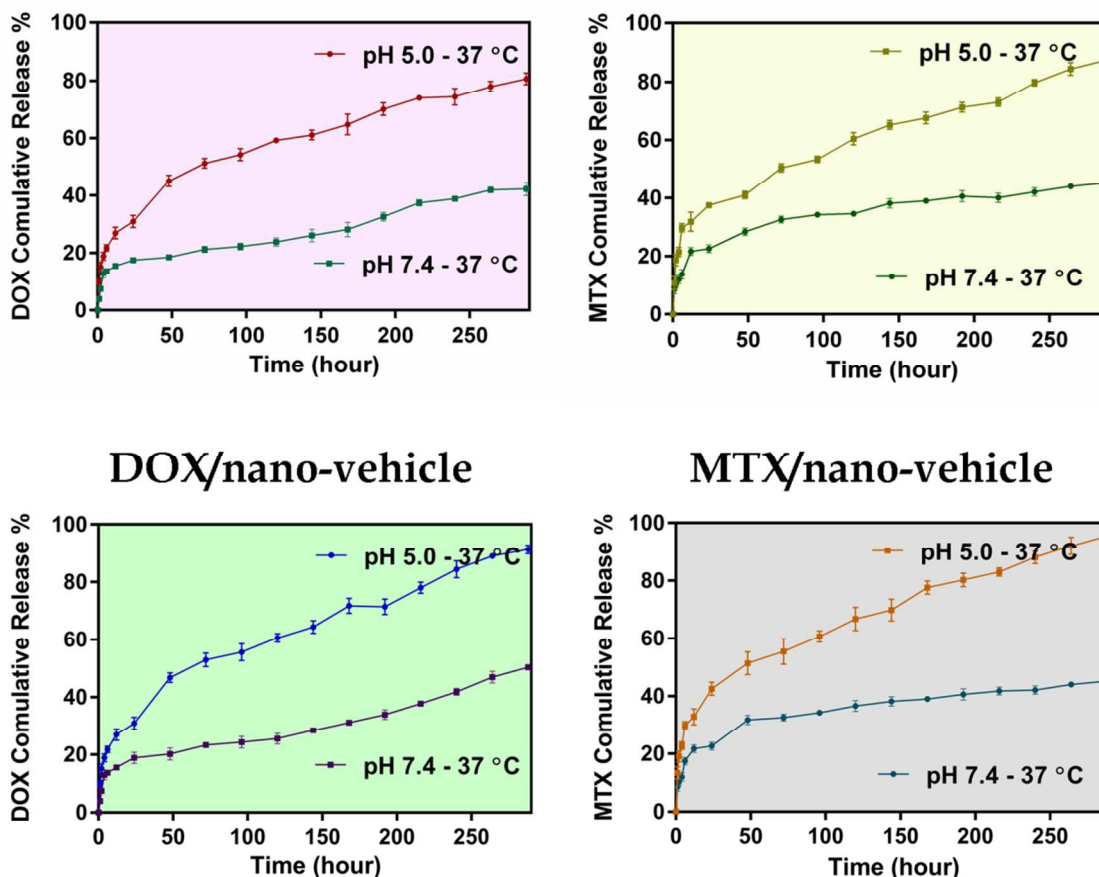


Figure 14: Cumulative release of DOX, and MTX of DOX/nano-vehicle, MTX-nano-vehicle, and DOX/MTX/nano-vehicle at various pH values (7.4 and 5.0) and 37 °C

3.7. Cytotoxicity study

The important key item regarding the drug carrier in drug delivery systems is their biocompatibility which is confirmed by the results of MTT assay (an approach extensively to evaluate the mitochondria activity to quantify the cell growth or cell death). Besides, the MTT assay was also conducted on MCF7 cells for comparing the cytotoxic effects of drugs-loaded nano-vehicle and free drugs (**Fig. 15**). After treating cells with nano-vehicle for 48 h, the results

were confirmed that the nano-vehicle has no significant cytotoxicity to the MCF7 cells with 95% cell viability (**Fig. 16**). Furthermore, the cytotoxicity of free DOX and MTX on MCF7 cells was studied and their inhibition concentrations (IC_{50}) in 48 h were obtained 7.22 and 9.52 $\mu\text{g mL}^{-1}$, respectively. The cytotoxic effect of DOX-MTX combination was also evaluated with IC_{50} value of 2.23 $\mu\text{g mL}^{-1}$ for 48 h. These results implied that combination DOX and MTX has more cytotoxic effect acting via two different mechanisms on MCF7 cancer cells death. Besides, the MCF7 cells were treated with DOX/MTX/nano-vehicle at the same drugs dosage to compare level of cytotoxicity with DOX/MTX. The IC_{50} of the DOX/MTX/nano-vehicle after treatment for 48 h was calculated 1.08 $\mu\text{g mL}^{-1}$ lower than their free drugs form.

After the evaluation of cytotoxicity assay, the combination effect analysis by CI was also calculated. $CI < 1$, $CI=1$, and $CI > 1$ indicate synergistic, additive, and antagonistic effects, respectively. The combination effects of DOX and MTX were calculated for all drugs dosage and reported under the MTT assay graph for each concentration. As the results were shown, combination of DOX and MTX in free forms have CI value about 0.96, 0.95, 1.01, 0.95, 0.82, and 0.94 for drug concentration of 0.25, 0.50, 1.00, 2.00, 4.00, and 8.00 $\mu\text{g mL}^{-1}$, respectively. However, combination treatment via DOX/MTX/nano-vehicle showed lower CI value in compared to free form (CI: 1.02, 0.99, 0.94, 0.95, 0.76, and 0.80). All data were confirmed that the combination treatment via DOX/MTX/nano-vehicle has synergistic effect by increasing the drugs concentration.

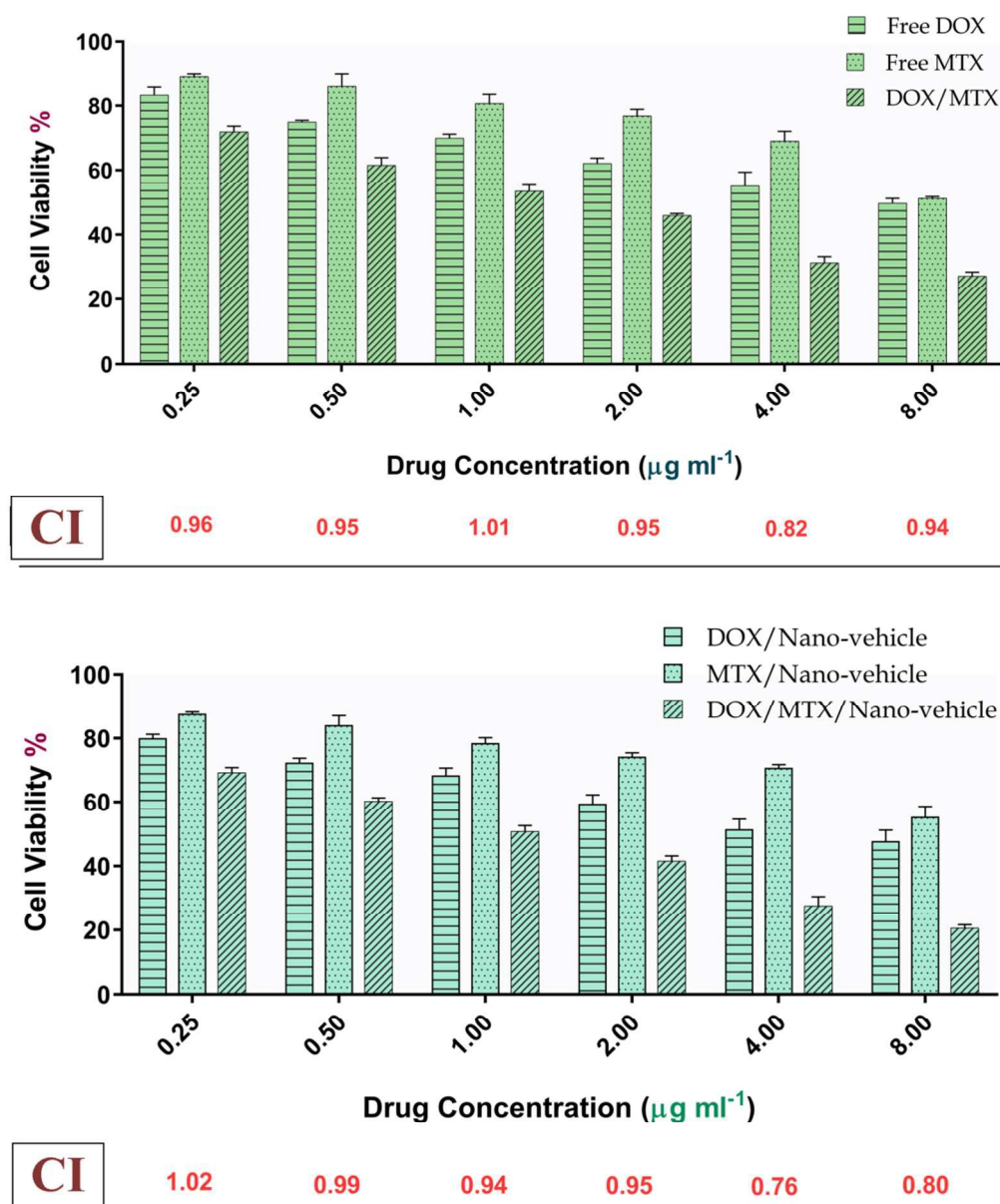


Figure 15: Cytotoxicity study of free DOX, free MTX, DOX/MTX, DOX/nano-vehicle, MTX/nano-vehicle, and DOX/MTX/nano-vehicle on MCF7 cells by MTT assay for 48 h

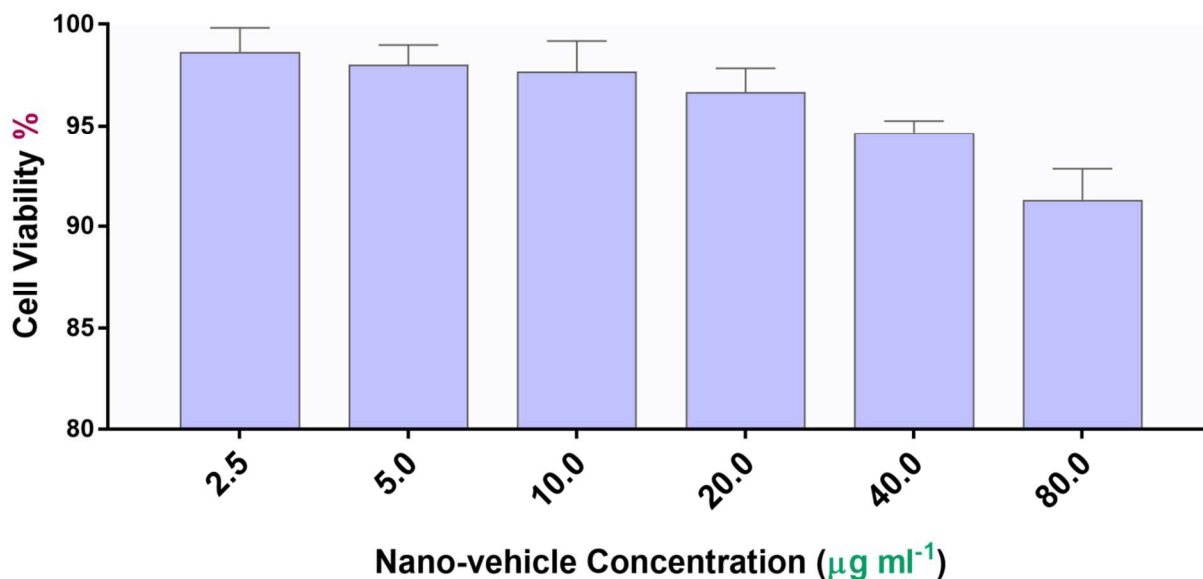


Fig. 16: Cytotoxic effects by MTT assay of blank nano-vehicle on MCF7 cells treated for 48 h

3.8. Targeted cellular uptake

To visualize the effect of human plasma protein-mediated endocytosis of nano-vehicle/pro in compared to bare nano-vehicle, the distribution of DOX-labelled nano-vehicle/pro and bare nano-vehicle on MCF7 cells was observed by flow-cytometry and fluorescent microscopy. MCF7 cells were treated with both and incubated for 2 h. Both samples show intracellular DOX concentration, which was visualized by the red intensity of DOX. As discussed in the SDS-PAGE assay section, many human plasma proteins have receptors on the cancer cells; therefore affinity of these proteins on the surface of nano-vehicle could help in the cellular uptake process. Our designed nano-vehicle has good affinity to the several proteins including transferrin, vitronectin, and apolipoprotein AI, albumin and etc. which was confirmed in the SDS-PAGE assay. The first three proteins have receptors on the surface of MCF7 cells and these facilitate the nano-vehicle to internalize the cancer cells. For this purpose, we designed a protocol for

evaluation of uptake percentage of both bare and nano-vehicle/pro and the cellular uptake was performed by flow-cytometry (**Fig. 17**). Interestingly, the results were shown that nano-vehicle/pro has more internalization to the MCF7 cells with 85.06% uptake percentage in compared to bare nano-vehicle with 70.15% uptake percentage. In second step, the fluorescent microscopy was used to validate our results. As seen in **Fig. 18**, there are no significant differences between both treated cells because this technique is a qualitative method. In overall, the flow-cytometry analysis was confirmed our hypothesis and it was concluded that our nano-vehicle could use for *in-vivo* applications with more efficiency.

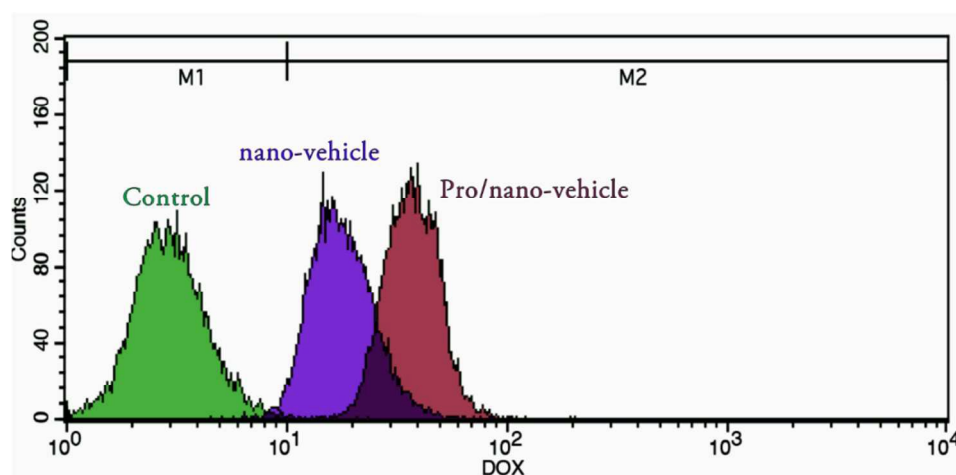


Figure 17: Study of targeted cell uptake by quantitative flow-cytometry analysis of cellular DOX red fluorescent of MCF7 cells incubated for 2 h

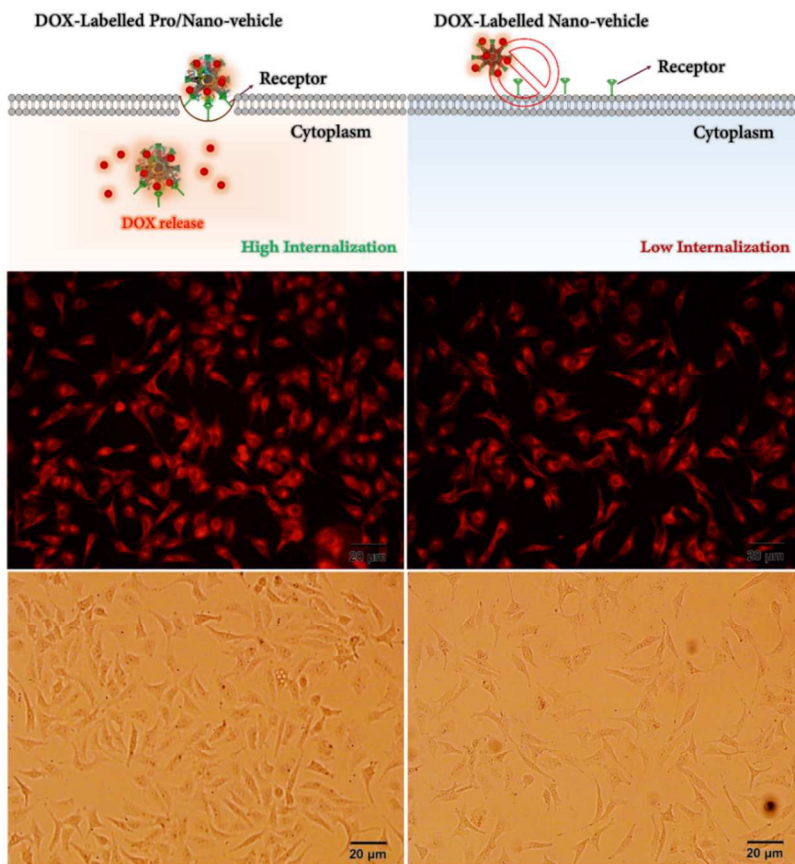


Figure 18: Cellular uptake of DOX-labelled nano-vehicle and DOX-labelled nano-vehicle/pro of MCF7 cells incubated for 2 h by fluorescent microscopy and schematic illustration of the uptake mechanism

3.9. Detection of apoptotic cells by DAPI staining

DAPI is a fluorescent agent which could bind strongly to A-T rich regions in DNA. It can pass through an intact cell membrane and be used to stain both live and fixed cell. In this regard, fluorescence microscopy was used to observe the morphological changes in MCF7 treated cells stained with DAPI for 48 h. As seen in **Fig. 19**, the cells with no treatment has homogenously shape, revealing that the chromatin was equally distributed in the nucleolus.⁴⁶ Beside, the treated cells with nano-vehicle showed no significant morphological changes in compared to the control.

By observing the treated cells with MTX, DOX, and DOX/MTX under fluorescence microscopy, the signal of apoptosis such as chromatin condensation, nucleolus pyknosis, and chromatin fragmentation was clearly observed.⁴⁷ By comparing these three groups, it was observed that DOX/MTX has very intense nuclear fragmentation of cells; however, the treated cells with both free DOX and free MTX also have drastic and high effects. However, the numbers of cells in combination drugs treatment (DOX-MTX) are lower than other two treatments with more drastic effects on the cancer cells. It was clear that the treated cells with DOX/MTX/nano-vehicle have significant effects on the cells nuclei and cytotoxic effects at the same drugs dosage like free combination drugs.

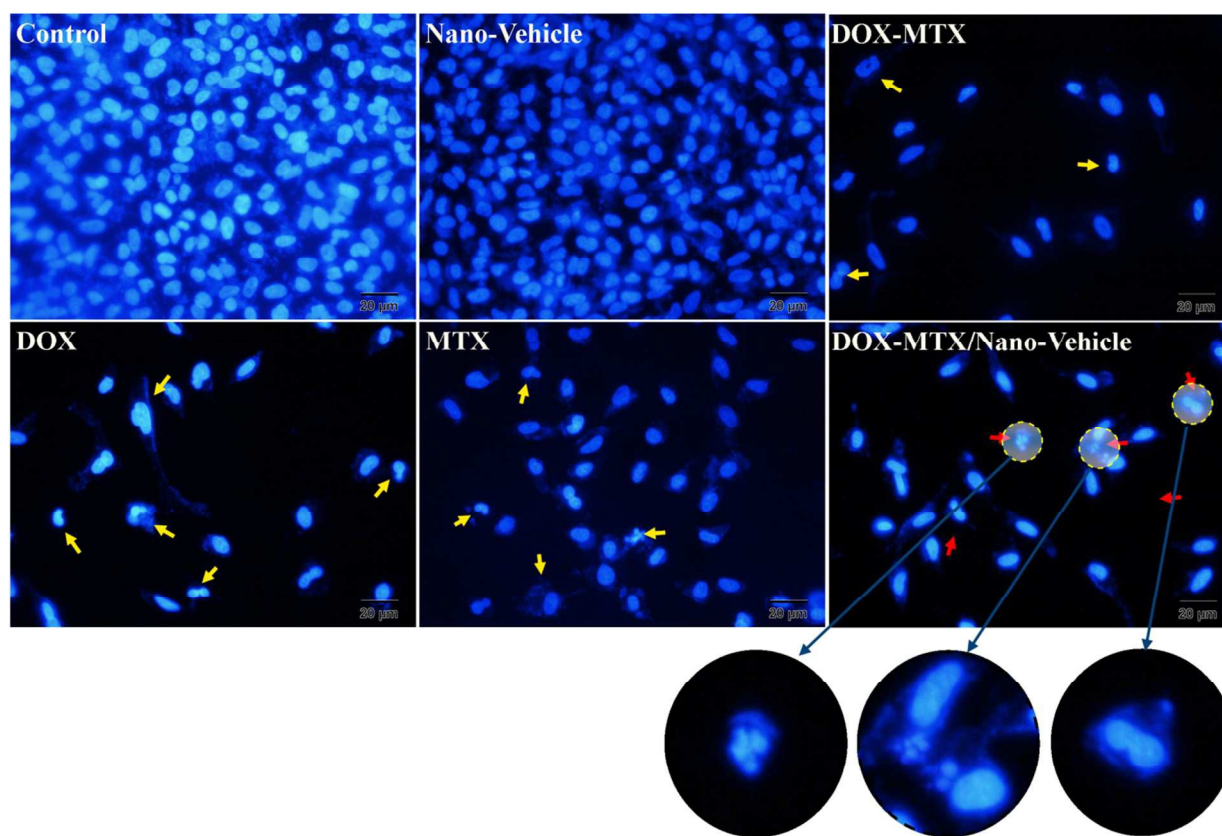


Figure 19: Fluorescence microscopy images of untreated and treated MCF7 cells (breast cancer cells), which have been stained with DAPI. The cells were stained with 5 mg mL^{-1} DAPI

solution after treatment for 48 h with nano-vehicle, free MTX, free DOX, DOX/MTX, and DOX/MTX/nano-vehicle. The cells with no treatment used as a control

4. Conclusion

In this study, we are endeavoring to develop a nano-vehicle, based on dendritic p-sulfonatocalix[4]arene as a dual-drug carrier for co-delivery of DOX and MTX to the MCF7 breast cancer cells with targeting and synergistic effects. The *in-vitro* cellular cytotoxicity test and hemolysis assay of blank nano-vehicle showed no significant cytotoxicity against MCF7 cell line and RBCs respectively. Hence, it could be used as a safe anticancer drug carrier. Furthermore, DOX/MTX/nano-vehicle showed a remarkably enhanced efficiency in killing the MCF7 cancer cells. SDS-PAGE assay results have shown that nano-vehicle as a drug carrier after intravenous injection could decorate with plasma proteins for enhancing nano-vehicle internalization to the MCF7 cancer cells. The cellular uptake by flow-cytometry was confirmed our hypothesis. To show our nano-vehicle enhanced efficiency in killing the MCF7 cancer cells, DAPI staining was also performed. All results persuade us that this nano-vehicle could be effectively used for cancer treatment and be used for further *in-vivo* applications.

Declaration of interest

The authors report no conflicts of interest.

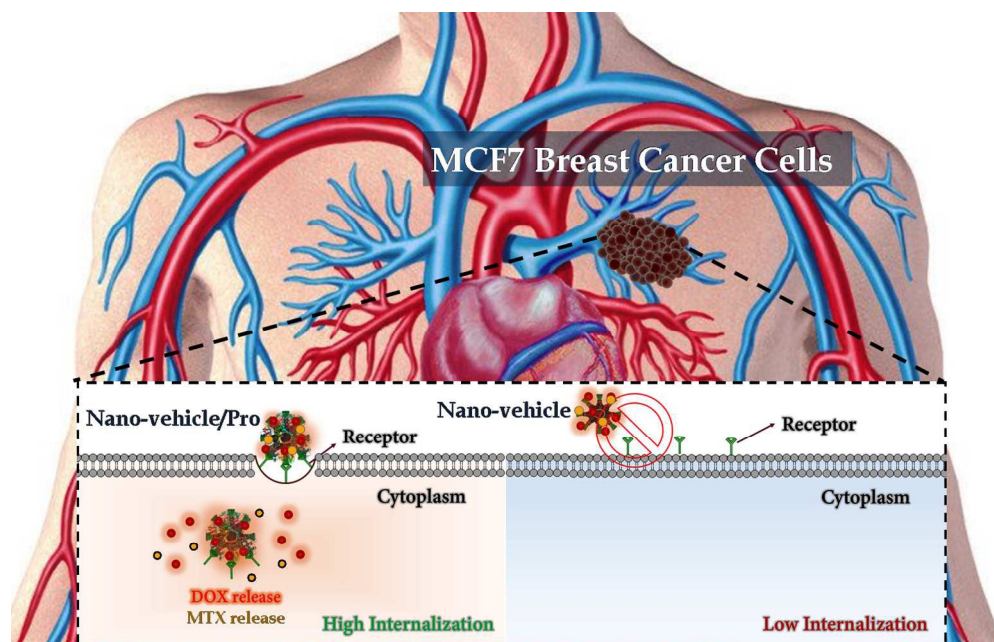
Acknowledgments

We thank of Drug Applied Research Center (DARC), Tabriz University of Medical Sciences, (Tabriz, Iran). All experiment in this report was done in DARC.

References

1. E. Ward, C. DeSantis, A. Robbins, B. Kohler and A. Jemal, *CA: a cancer journal for clinicians*, 2014, **64**, 83-103.
2. C. E. DeSantis, C. C. Lin, A. B. Mariotto, R. L. Siegel, K. D. Stein, J. L. Kramer, R. Alteri, A. S. Robbins and A. Jemal, *CA: a cancer journal for clinicians*, 2014, **64**, 252-271.
3. R. Siegel, J. Ma, Z. Zou and A. Jemal, *CA: a cancer journal for clinicians*, 2014, **64**, 9-29.
4. R. A. Burrell, N. McGranahan, J. Bartek and C. Swanton, *Nature*, 2013, **501**, 338.
5. F. B. zeynabad, R. Salehi, E. Alizadeh, H. S. Kafil, A. Hassanzadeh and M. Mahkam, *RSC advances*, 2015, **5**, 105678-105691.
6. P. Gholizadeh, H. Eslami, M. Yousefi, M. Asgharzadeh, M. Aghazadeh and H. S. Kafil, *Biomed Pharmacother*, 2016, **84**, 552-558.
7. T. Assi, E. El Rassy, S. Tabchi, T. Ibrahim, T. Moussa, R. Chebib, F. El Karak, F. Farhat, G. Chahine and F. Nasr, *Supportive Care in Cancer*, 2016, **24**, 1603-1608.
8. E. B. C. T. C. Group, *The Lancet*, 2005, **366**, 2087-2106.
9. T. E. Sharp III and J. C. George, *Frontiers in oncology*, 2014, **4**, 299.
10. N. D. James, M. R. Sydes, N. W. Clarke, M. D. Mason, D. P. Dearnaley, M. R. Spears, A. W. Ritchie, C. C. Parker, J. M. Russell and G. Attard, *The Lancet*, 2016, **387**, 1163-1177.
11. V. Shafiei-Irannejad, N. Samadi, R. Salehi, B. Yousefi and N. Zarghami, *Chemical biology & drug design*, 2017, **90**, 1056-1066.
12. L. Li, W. Gu, J. Chen, W. Chen and Z. P. Xu, *Biomaterials*, 2014, **35**, 3331-3339.
13. S. Z. Vahed, R. Salehi, S. Davaran and S. Sharifi, *Materials Science and Engineering: C*, 2017, **71**, 1327-1341.
14. V. Shafiei-Irannejad, N. Samadi, B. Yousefi, R. Salehi, K. Velaei and N. Zarghami, *Chemical biology & drug design*, 2018, **91**, 269-276.
15. H. Zhu, H. Chen, X. Zeng, Z. Wang, X. Zhang, Y. Wu, Y. Gao, J. Zhang, K. Liu and R. Liu, *Biomaterials*, 2014, **35**, 2391-2400.
16. V. Shafiei-Irannejad, N. Samadi, R. Salehi, B. Yousefi, M. Rahimi, A. Akbarzadeh and N. Zarghami, *Pharmaceutical research*, 2018, **35**, 119.
17. M. Afsharzadeh, M. Hashemi, A. Mokhtarzadeh, K. Abnous and M. Ramezani, *Artificial cells, nanomedicine, and biotechnology*, 2017, 1-16.
18. S. Gadde, *MedChemComm*, 2015, **6**, 1916-1929.
19. J. Liu, C. Wang, X. Wang, X. Wang, L. Cheng, Y. Li and Z. Liu, *Advanced Functional Materials*, 2015, **25**, 384-392.
20. R. Salehi, K. Nowruzi, S. Salehi, A. A. Khandaghi, S. Davaran and A. A. Entezami, *International Journal of Polymeric Materials and Polymeric Biomaterials*, 2013, **62**, 686-694.
21. R. Salehi, K. Nowruzi, A. Entezami, V. Asgharzadeh and S. Davaran, *Polymers for Advanced Technologies*, 2009, **20**, 416-422.
22. Z. Li, L. Zhang, C. Tang and C. Yin, *Pharmaceutical research*, 2017, **34**, 2829-2841.

23. P. Kesharwani and A. K. Iyer, *Drug discovery today*, 2015, **20**, 536-547.
24. S. J. Sonawane, R. S. Kalhapure, S. Rambharose, C. Mocktar, S. B. Vepuri, M. Soliman and T. Govender, *International journal of pharmaceuticals*, 2016, **504**, 1-10.
25. O. Tacar, P. Sriamornsak and C. R. Dass, *Journal of Pharmacy and Pharmacology*, 2013, **65**, 157-170.
26. H. He, Y. Wang, H. Wen and X. Jia, *RSC Advances*, 2014, **4**, 3643-3652.
27. Y. Zhang, C. Yang, W. Wang, J. Liu, Q. Liu, F. Huang, L. Chu, H. Gao, C. Li and D. Kong, *Scientific reports*, 2016, **6**.
28. W. T. Purcell and D. S. Ettinger, *Current oncology reports*, 2003, **5**, 114-125.
29. J. Chen, L. Huang, H. Lai, C. Lu, M. Fang, Q. Zhang and X. Luo, *Molecular pharmaceuticals*, 2013, **11**, 2213-2223.
30. M. Rahimi, K. D. Safa, E. Alizadeh and R. Salehi, *New Journal of Chemistry*, 2017, **41**, 3177-3189.
31. C. D. Gutsche, B. Dhawan, K. H. No and R. Muthukrishnan, *Journal of the American Chemical Society*, 1981, **103**, 3782-3792.
32. D. Xiong, M. Chen and H. Li, *Chemical Communications*, 2008, 880-882.
33. K. A. Mahmoud, J. A. Mena, K. B. Male, S. Hrapovic, A. Kamen and J. H. Luong, *ACS applied materials & interfaces*, 2010, **2**, 2924-2932.
34. E. Kaiser, R. Colescott, C. Bossinger and P. Cook, *Analytical biochemistry*, 1970, **34**, 595-598.
35. B. Chertok, A. E. David and V. C. Yang, *Biomaterials*, 2010, **31**, 6317-6324.
36. J. Yang, Y. Liu, H. Wang, L. Liu, W. Wang, C. Wang, Q. Wang and W. Liu, *Biomaterials*, 2012, **33**, 604-613.
37. N. S. Rejinold, M. Muthunarayanan, V. Divyarani, P. Sreerekha, K. Chennazhi, S. Nair, H. Tamura and R. Jayakumar, *Journal of colloid and interface science*, 2011, **360**, 39-51.
38. T.-C. Chou, *Pharmacological reviews*, 2006, **58**, 621-681.
39. M. Rahimi, S. Shojaei, K. D. Safa, Z. Ghasemi, R. Salehi, B. Yousefi and V. Shafiei-Irannejad, *New Journal of Chemistry*, 2017, **41**, 2160-2168.
40. J. Zhang, W. Sun, L. Bergman, J. M. Rosenholm, M. Lindén, G. Wu, H. Xu and H.-c. Gu, *Materials Letters*, 2012, **67**, 379-382.
41. U. FDA, 2005.
42. Y. Zhou, J. Li, F. Lu, J. Deng, J. Zhang, P. Fang, X. Peng and S.-F. Zhou, *Drug design, development and therapy*, 2015, **9**, 2635.
43. C. Corbo, R. Molinaro, A. Parodi, N. E. Toledano Furman, F. Salvatore and E. Tasciotti, *Nanomedicine*, 2016, **11**, 81-100.
44. S. Tenzer, D. Docter, S. Rosfa, A. Wlodarski, J. r. Kuharev, A. Rekić, S. K. Knauer, C. Bantz, T. Nawroth and C. Bier, *ACS nano*, 2011, **5**, 7155-7167.
45. M. Rahimi, K. D. Safa and R. Salehi, *Polymer Chemistry*, 2017, **8**, 7333-7350.
46. P. Xu, H. Zuo, B. Chen, R. Wang, A. Ahmed, Y. Hu and J. Ouyang, *Scientific reports*, 2017, **7**, 42632.
47. M. Rahimi, V. Shafiei-Irannejad, K. D. Safa and R. Salehi, *Carbohydrate Polymers*, 2018, **196**, 299-312.



145x92mm (300 x 300 DPI)